



Synthesis, biological evaluation and molecular modeling of novel selective COX-2 inhibitors: sulfide, sulfoxide, and sulfone derivatives of 1,5-diarylpyrrol-3-substituted scaffold



Annalisa Reale^a, Simone Brogi^b, Alessia Chelini^a, Marco Paolino^a, Angela Di Capua^{a,f}, Germano Giuliani^a, Andrea Cappelli^a, Gianluca Giorgi^a, Giulia Chemi^a, Alessandro Grillo^a, Massimo Valoti^c, Lidia Sautebin^d, Antonietta Rossi^d, Simona Pace^{d,g}, Concettina La Motta^b, Lorenzo Di Cesare Mannelli^e, Elena Lucarini^e, Carla Ghelardini^e, Maurizio Anzini^{a,*}

^a Dipartimento di Biotecnologie, Chimica e Farmacia, (Dipartimento d' Eccellenza 2018-2022), Università di Siena, Via A. Moro, I-53100 Siena, Italy

^b Dipartimento di Farmacia, Università di Pisa, Via Bonanno 6, I-56126 Pisa, Italy

^c Dipartimento di Scienze della Vita, Università di Siena, Via A. Moro, I-53100 Siena, Italy

^d Dipartimento di Farmacia, (Dipartimento d' Eccellenza 2018-2022), Scuola di Medicina e Chirurgia, Università di Napoli "Federico II", Via D. Montesano 49, I-80131 Napoli, Italy

^e Dipartimento di Neuroscienze, Area del Farmaco e Salute del Bambino (NEUROFARBA), Università di Firenze, Viale G. Pieraccini 6, I-50139 Firenze, Italy

ARTICLE INFO

Keywords:

COX-2 inhibitors
1,5-Diarylpyrrole derivatives
Anti-inflammatory agents
Antinociceptive agents
Molecular modeling

ABSTRACT

A novel series of 1,5-diarylpyrrol-3-sulfur derivatives (**10–12**) was synthesized and characterized by NMR and mass spectroscopy and x-ray diffraction. The biological activity of these compounds was evaluated *in vitro* and *in vivo* tests to assess their COX-2 inhibitory activity along with anti-inflammatory and antinociceptive effect.

Results showed that the bioisosteric transformation of previously reported alkoxyethyl ethers (**9a–c**) into the corresponding alkyl thioethers (**10a–c**) still leads to selective and active compounds being the COX-2 inhibitory activity for most of them in the low nanomolar range. The oxidation products of **10a,b** were also investigated and both couple of sulfoxides (**11a,b**) and sulfones (**12a,b**) showed an appreciable COX-2 inhibitory activity. Molecular modeling studies were performed to investigate the binding mode of the representative compounds **10b**, **11b**, and **12b** into COX-2 enzyme and to explore the potential site of metabolism of **10a** and **10b** due to the different *in vivo* efficacy. Among the developed compounds, compound **10b** showed a significant *in vivo* anti-inflammatory and antinociceptive activity paving the way to develop novel anti-inflammatory drugs.

1. Introduction

Agents able to selectively inhibit cyclooxygenase-2 (COX-2) are currently used for an effective treatment of inflammatory diseases such as rheumatoid arthritis (RA) and osteoarthritis (OA).^{1,2} Several studies have recently demonstrated that selective COX-2 inhibitors can also induce apoptosis in colon, stomach, prostate and breast cancer cell lines.^{3–7} Furthermore, selective COX-2 inhibitors offer potential for the prophylactic prevention of inflammatory neurodegenerative disorders such as Alzheimer's disease.⁸

Due to their satisfactory therapeutic profile, selective COX-2 inhibitors represent a step forward when compared to traditional

nonsteroidal anti-inflammatory agent (tNSAIDs) being devoid of gastrointestinal adverse effects (gastritis, ulcers, bleeding) typical of this class of drugs (e.g. acetylsalicylic acid, diclofenac, indomethacin, etc.).⁹ In fact, manipulation of indomethacin structure (**1**) (Figure 1) by applying the "scaffold hopping approach",¹⁰ led to the first selective COX-2 inhibitory compound DuP 697 (**2**) as the prototype, based on the diaryl heterocyclic structure. This compound served as the rationale for the original concept that a drug endowed with greater selectivity for the pro-inflammatory inducible COX-2 isozyme, relative to the cytoprotective constitutive COX-1 isozyme, would have reduced the incidence of gastrointestinal bleeding. Subsequent drug discovery programs led to the clinical development of a new class of anti-inflammatory drugs

* Corresponding author.

E-mail address: maurizio.anzini@unisi.it (M. Anzini).

^f Present address: Department of Chemistry and Biochemistry, The Ohio State University, Columbus, Ohio 43210, United States.

^g Present address: Department of Pharmaceutical/Medicinal Chemistry, Institute of Pharmacy, Friedrich-Schiller-University, Jena, Germany.

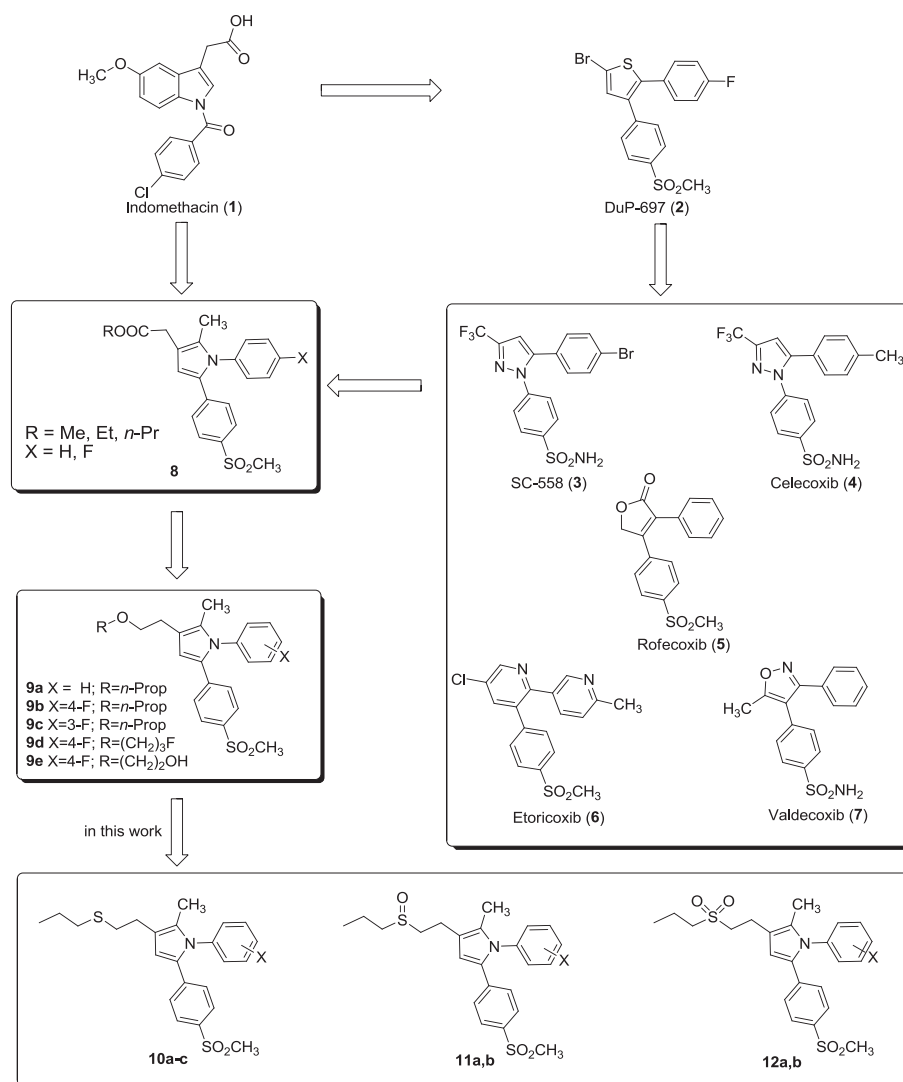


Figure 1. From tNSAIDs to coxibs: structures of indomethacin (1), reference compounds (2–7), 1,5-diarylpyrrole-3 substituted derivatives (8, 9) and development of novel selective COX-2 tio-inhibitors.

referred to as coxibs, in which vicinal diaryl heterocycles constitute the major class of selective COX-2 inhibitors such as SC-558 (3), celecoxib (4), rofecoxib (5), etoricoxib (6), and valdecoxib (7). In this regard, all the compounds cited above differ from the central heterocyclic core: celecoxib (4) possesses a central five-membered pyrazole ring, whereas etoricoxib (6) has a central six-membered pyridine ring.^{11,12} Another highly selective COX-2 inhibitor rofecoxib (5), which belongs to the diaryl heterocyclic class possesses a central five-member lactone, [2(5H) furanone], ring system while valdecoxib (7) is based on an isooxazole ring.¹³ Extensive structure–activity relationship (SAR) studies for the diaryl heterocyclic class have shown that a sulfonamide (SO₂NH₂) or a methyl sulfone (SO₂Me) and fluoro substituents at the *para* position of one of the aryl rings often provides optimum COX-2 selectivity and potency.¹⁴

Unfortunately, it was found that the gastrointestinal benefit of coxibs is frustrated by the finding of increased incidence of undesirable cardiovascular side-effects.¹⁵ However, according to the evidences of different observational studies and randomized clinical trials the cardiovascular hazard is not restricted to selective COX-2 inhibitors but also to some tNSAIDs, such as diclofenac.¹⁶ The most plausible mechanism is the suppression of COX-2-dependent prostacyclin, leaving unconstrained the intricate network of stimuli predisposing to atherogenesis, hypertension, and thrombosis, such as Thromboxane

(TxA₂).¹⁷ The finding of a marked variability in how each person reacts to these drugs,¹⁸ encouraged the development of novel compounds in order to increase the spectrum of therapeutic opportunities for each individual patient.

Thus, more than a decade ago we started a wide research program focused on the synthesis of 3-substituted-1,5-diarylpyrrole derivatives (8)^{19,20} as new selective COX-2 inhibitors in which the pyrroleacetic and vicinal diaryl heterocyclic moieties were reminiscent of indomethacin (1) and of the above “coxib” family, respectively.

Further functionalization of the chain in position 3 of the pyrrole moiety allowed us to enlarge the library of previously reported compounds (8) with a small series of 1,5-diarylpyrrole-3-alkoxyethyl ethers (9).²¹ Among these, the hydroxyethyl derivatives (R = CH₂CH₂OH in Figure 1) were disclosed when the research project was extended to the synthesis of hybrid molecules, essentially new classes of pyrrole-derived nitroxyalkyl inverse esters,²² and ethers as COX-2 selective inhibitors/nitric oxide (NO) donors also referred to as CINOD (Figure 1).²³

In the *in vitro* cell culture assay, all the compounds proved to be potent and selective COX-2 inhibitors. In the human whole blood (HWB) assay, compound 9a (X = H, R = *n*-Pr, see Table 1 for the exact structure) had a comparable COX-2 selectivity to valdecoxib, while it was more selective than celecoxib but less selective than rofecoxib. The potential anti-inflammatory and antinociceptive activities of

Table 1

Biological activity of target compounds **10–12** in comparison with that of previously reported alkoxyethyl ethers **9a–d**, and hydroxyethyl ether **9e**.

Cmpd	X	R	IC ₅₀ COX-1 (μM) ^a	IC ₅₀ COX-2 (μM) ^a	COX-1/COX-2 (SI) ^b
9a^c	H	<i>n</i> -Pr	> 100	0.018	> 5555
9b^c	4-F	<i>n</i> -Pr	> 100	0.030	> 3333
9c^c	3-F	<i>n</i> -Pr	> 100	0.013	> 7692
9d^d	4-F	(CH ₂) ₃ F	> 100	0.007	> 14.285
9e^e	4-F	(CH ₂) ₂ OH	> 10	0.089	> 112.3
10a	H	<i>n</i> -Pr	> 10	0.014	> 714
10b	4-F	<i>n</i> -Pr	> 10	0.011	> 909
10c	3-F	<i>n</i> -Pr	> 10	0.285	> 24
11a	H	<i>n</i> -Pr	> 10	0.060	> 167
11b	4-F	<i>n</i> -Pr	> 10	0.040	> 250
12a	H	<i>n</i> -Pr	> 10	0.034	> 294
12b	4-F	<i>n</i> -Pr	> 10	0.044	> 227
Celecoxib^d	–	–	5.1	0.079	65

^a Results are expressed as the mean (n = 3 experiments) of the % inhibition of PGE₂ production by test compounds with respect to control samples. The IC₅₀ values were calculated by the GraphPad Instat program. Data fit was obtained by means of the sigmoidal dose–response equation (variable slope) (GraphPad software).

^b *In vitro* COX-2 selectivity index [IC₅₀(COX-1)/IC₅₀(COX-2)].

^c See reference [21].

^d See reference [26].

compounds **9a** and **9b** (X = F, R = *n*-Pr, see [Table 1](#) for the exact structure) were evaluated *in vivo*, where they showed a very good activity against both carrageenan-induced hyperalgesia and oedema in the rat paw test. In the abdominal constriction test compounds **9a** and **9b** were able to reduce the number of writhes in a statistically significant manner.²¹

Compound **9a** was also evaluated to assess its effect on human osteoarthritic chondrocytes exposed to Interleukin(IL)-1β showing a beneficial effect on chondrocytes metabolism.²⁴ In addition, when tested to evaluate their antiproliferative activity in the HaCaT (aneuploid immortal keratinocytes from adult human skin), compounds **9a** and **9b** showed a strong inhibition of cell proliferation and did not exhibit cytotoxicity.²⁵ The research continued with the synthesis of different fluorinated 1,5-diarylpyrrole-3-alkoxyethyl ether derivatives with the aim of investigating the biological effects that could have been elicited by insertion of a fluorine atom in a different portion of the previously synthesized COX-2 inhibitors.²⁶ Among them, compound **9d** exhibited a prominent *in vivo* anti-inflammatory and antinociceptive activities, also confirming the antiproliferative but not toxic effect on HaCaT cell of this class of compounds ([Figure 1](#)).²⁶ These data suggested that compounds **9a–d** along with their role in inhibiting COX-2 and inflammation, could have a possible therapeutic (topical or systemic) use against skin proliferative disorders, such as psoriasis.

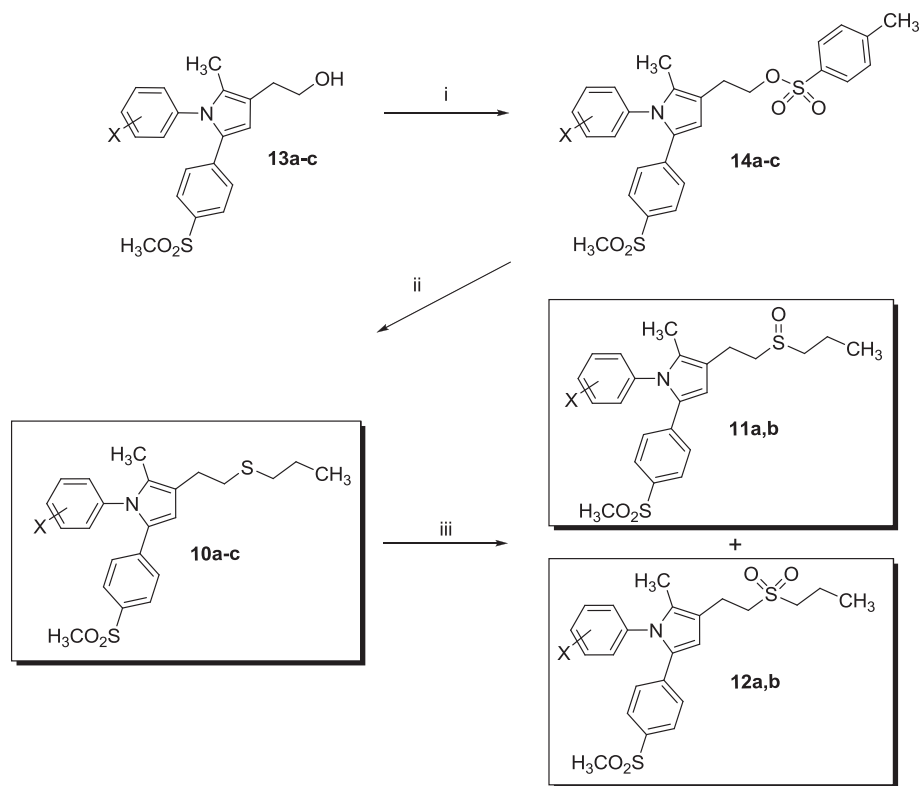
As for hydroxyethyl derivative **9e** (X = F, R = CH₂CH₂OH, see [Table 1](#) for the exact structure), as well as compounds **9a–d**, it demonstrated an appreciable anti-inflammatory and antinociceptive activity in animal models of inflammation and for this reason underwent biological assays performed on bovine articular cartilage, in which **9e** proved to be endowed with chondroprotective effects being able to inhibit glycosaminoglycans release induced by IL-1β.²³

Very recently, compound **9e** was also found to have more beneficial effect compared with celecoxib with special regard to the modulation of oxidation/anti-oxidant system and proteasome profile of human articular chondrocytes.²⁷

In this work, following the strategy of bioisosterism, a hitherto unknown series of 1,5-diarylpyrrole-3-sulfur derivatives (**10–12**) was synthesized, the biological activity of which was evaluated in *in vitro* and *in vivo* test to assess their inhibitory COX-2 activity along with anti-inflammatory and antinociceptive effect.

2. Results and discussion

As a third row element sulfur is able to expand its valence shell to form more than four covalent bonds assuming different oxidation states ranging from – 2 to + 6 that allow this atom to assume a variety of molecular arrangements, making it one of the most chemically versatile



Scheme 1. Synthesis of the new COX-2 inhibitors **10a-c**, **11a,b** and **12a,b**. Reagents and conditions: (i) TsCl, DMAP, DIPEA, DCM, r.t., 20 h; (ii) sodium 1-propanthiolate, dry DMSO, r.t., 1 h; (iii) mCPBA, DCM, 2 h, r.t.

Table 2

Effect of compounds **10a-c**, and **11b** on hyperalgesia and edema induced by carrageenan in the rat paw-pressure test.^a

Pre-treatment i.pl.	Treatment p.o.	Dose (mg Kg ⁻¹)	Paw Pressure (g)				Paw Volume (mL)
			Before Treatment	After Treatment			30 min.
				30 min.	60 min.	90 min.	
Saline	CMC	–	60.2 ± 2.7	59.3 ± 2.5	62.8 ± 3.3	60.5 ± 4.4	1.59 ± 0.08
Carrageenan	CMC	–	35.4 ± 3.8	33.9 ± 3.7	37.2 ± 3.5	36.7 ± 4.0	2.78 ± 0.09
Carrageenan	10^o	20	36.7 ± 4.7	46.0 ± 4.0*	40.3 ± 3.5	40.2 ± 3.8	1.69 ± 0.10*
Carrageenan	10b	20	34.8 ± 3.8	57.3 ± 4.2*	50.4 ± 4.0*	41.9 ± 4.0	1.75 ± 0.09*
Carrageenan	10c	20	37.9 ± 4.3	41.5 ± 3.1*	38.8 ± 3.4	37.2 ± 3.1	1.74 ± 0.07*
Carrageenan	11b	20	35.6 ± 3.9	53.5 ± 4.1*	42.5 ± 3.6	38.2 ± 3.7	1.55 ± 0.07*

^a All compounds were administered at the dose of 20 mg kg⁻¹ p.o. Carrageenan (100 µL – 1% - i.pl. 2 h before test). Test was performed 30 min after the compound injection. There were 4–5 rats per group. *P < 0.05 versus the corresponding carrageenan-treated rat; *P < 0.01 versus the corresponding carrageenan-treated rat.

of the early elements.²⁸ Many compounds and marketed drugs endowed with biological activity include the S-linker comprising sulfide (R-S-R'), sulfinyl (R-S(O)-R') and sulfonyl R-(SO₂)-R' groups²⁹ [e.g. montelukast, esomeprazole, and amisulpiride, respectively]. Therefore, the transformation of previously reported pyrrole 1,5-diarylpyrrole-3-substituted alkoxyethyl ethers as highly selective COX-2 inhibitors **9a-c**^{21,26} into the bioisosteric sulfur-containing homologues, could be conceived as a further functionalization of position 3 of the pyrrole scaffold. Moreover, operating in this direction, it appeared obvious to investigate their oxidation products such as alkyl sulfoxides and alkyl sulfones. In fact, all three species of sulfur derivatives are present in the pharmacokinetic pathway of well-known drugs like non-steroidal anti-inflammatory agent (NSAID) sulindac in which the inactive sulfoxide undergoes either reduction to the active sulfide metabolite or irreversible oxidation to sulindac sulfone,³⁰ differently from the antigout agent sulfapyrazone in which the sulfoxide is the active compound while the sulfide and the sulfone are the inactive metabolites.³¹

2.1. Chemistry

The synthesis of the designed compounds is reported in Scheme 1. Initially, the hydroxyethyl derivatives **13a-c** were prepared in gram-scale according to the previously-reported procedure.²¹ The activation of the suitable alcohol **13a-c** by means of tosyl chloride in the presence of *N,N*-diisopropylethylamine (DIPEA) and 4-(dimethylamino)pyridine (DMAP) gave the corresponding O-tosyl derivatives **14a-c** which were smoothly alkylated by reaction with sodium 1-propanthiolate in dimethylsulfoxide (DMSO) at room temperature to provide alkyl sulfides also referred to as thioethers, **10a-c** in satisfactory yields.³²

Sulfoxides and sulfones are generally prepared by mono or full oxidation of sulfides and the chemoselectivity of the oxidation depends on the reaction conditions, amount of oxidizing agent, typically hydrogen peroxide and the use of a promoter like triflic anhydride or molybdenum(VI) oxide.³³

Surprisingly, the chemoselective oxidation of sulfides **10a,b** to obtain sulfoxides **11a,b** and sulfones **12a,b** following the above-cited

Table 3
Effect of compounds **10a-c**, and **11b** in the mouse abdominal constriction test (acetic acid 0.6%).

Treatment ^a	n° mice	DOSE per os (mg Kg ⁻¹)	n° writhes
CMC	12	–	30.5 ± 3.7
10a	5	10	32.6 ± 3.9
10a	5	20	25.9 ± 3.2 [†]
10a	5	40	26.4 ± 3.0 [†]
10b	5	10	28.7 ± 4.1
10b	5	20	17.4 ± 2.5 [*]
10b	5	40	15.9 ± 3.6 [*]
10c	5	10	30.3 ± 3.5
10c	5	20	23.4 ± 3.0 [†]
10c	5	40	23.7 ± 3.3 [†]
11b	5	10	28.8 ± 3.3 [†]
11b	5	20	23.4 ± 3.0 [†]
11b	5	40	20.3 ± 3.8 [†]

^a All drugs were administered *per os* 30 min before test. [†]P < 0.05 vs vehicle-treated mice; ^{*}P < 0.05 vs vehicle-treated mice.

conditions was unsuccessful obtaining complex reaction mixtures. Therefore, we decided to selectively oxidize sulfides **10a,b** by means of *meta*-chloroperoxybenzoic acid (*m*CPBA) in dry dichloromethane.³⁴ In this condition, we obtained sulfoxides **11a,b** as the main products (about 60% of yield) and sulfones **12a,b** as by-product (about 10% of yield). Sulfoxides and sulfones were easily separated by flash chromatography, characterized, and used for *in vitro* and *in vivo* biological evaluation.

2.2. *In vitro* assay

The inhibitory potency and selectivity on both COX-isoforms of the title compounds was evaluated by *in vitro* cell culture (J774 murine macrophage) assay. The results were summarized in Table 1 and

compared with some previously reported analogues alkoxyethyl ether compounds.

Results showed that the bioisosteric transformation of alkoxyethyl ethers **9a-c** into the corresponding alkyl thioethers (**10a-c**) still leads to selective and active compounds being the COX-2 inhibitory activity for most of them in the low nanomolar range. In particular, no significant difference between oxygen or sulfur linker were observed comparing **9a** (IC₅₀ = 0.018 μM) and **10a** (IC₅₀ = 0.014 μM). In the same way, elevated COX-2 inhibitory and selective effect was observed when a fluoro substituent in the *para* position of the pendant N-1 phenyl ring was inserted as in **9b** (IC₅₀ = 0.030 μM) and **10b** (IC₅₀ = 0.011 μM). Therefore, in the 3-substituted-1,5-diarylpyrrole series the contemporary presence of the propyl sulfide moiety and 4'-fluoro substituent as in **10b** represents the best combination to elicit a potent and selective COX-2 inhibitory activity. On the contrary, a significant loss of inhibitory activity on COX-2 was observed transforming compound **9c** into the analogue thioether **10c**.

On the basis of the promising inhibitory activity data obtained with thioether compounds **10a,b**, we investigated the inhibitory activity on both COX isoforms of compounds **11a,b** and **12a,b** considered as possible products of metabolic oxidation of the most active thioether derivatives. Both couple of sulfoxides **11a,b** and sulfones **12a,b** showed an appreciable COX-2 inhibitory activity with an IC₅₀ between 0.034 and 0.060 μM. These data suggest that even the oxidation products of propyl sulfides **10a,b** retain an intriguing COX-2 inhibitory activity regardless of the presence of the fluorine atom in *para* position of the pendant N-1 phenyl ring.

Intriguingly, sulfoxide **11a,b** and sulfones **12a,b** show similar nanomolar COX-inhibitory activity in the range of the alkoxyethyl ethers **9**. This observation suggests that the oxygen atom in the oxidized sulfur derivatives (at least one in the sulfones) may be involved in productive interactions analogously to the oxygen atom present in the side chain of compounds **9**, implicated in hydrogen bonds with the guanidine moiety

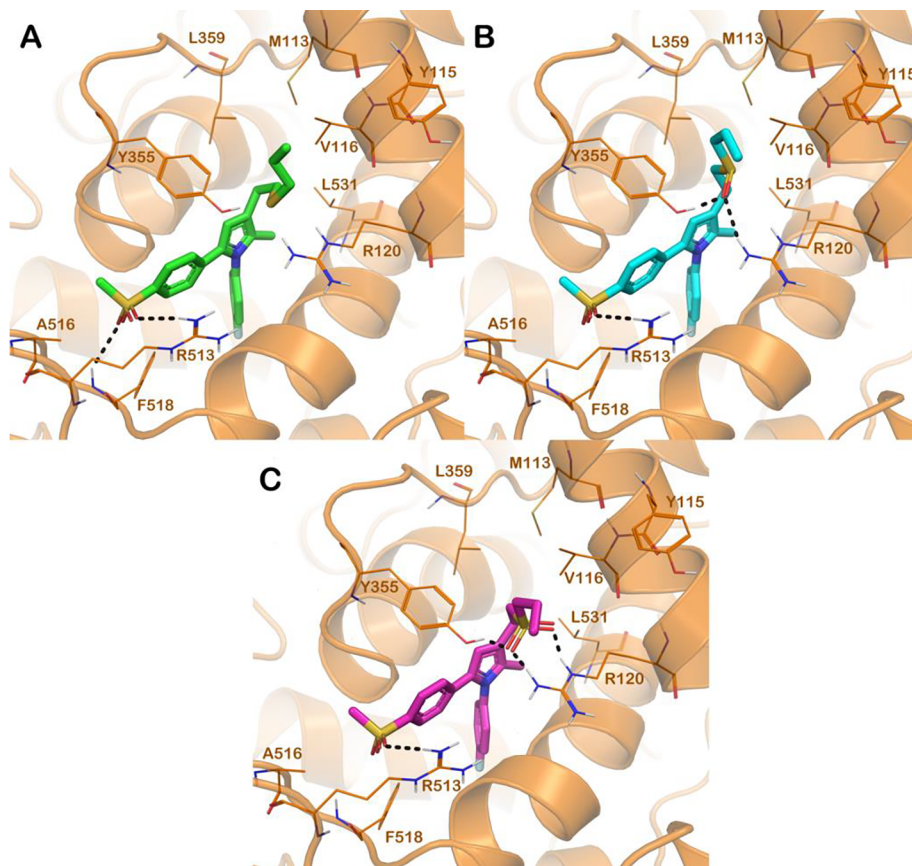


Figure 2. Best docked poses of compounds **10b** (panel A; green sticks), **11b** (panel B; cyan sticks) and **12b** (panel C; magenta sticks) into *h*COX-2 (orange cartoon PDB ID: 5KIR) binding site. The key residues in the active site were represented by lines. H-bonds were represented by dark grey dotted lines. The nonpolar hydrogens were omitted for the sake of clarity. The picture was generated by means of PyMOL (The PyMOL Molecular Graphics System, version 1.8.4.0, Schrödinger, LLC, New York, 2018).

of R120 and/or Y355 located in hydrophobic environment of the COX-2 “carboxylate binding site”.²¹

2.3. *In vivo* anti-inflammatory and antinociceptive studies

On the basis of their interesting COX-2 inhibitory activity observed in the *in vitro* test, compounds **10a-c**, together with compound **11b** (considered as the oxidation product of the most potent thioether compound **10b**) were selected as candidates for further pharmacological test to assess their *in vivo* anti-inflammatory and antinociceptive activities by carrying out the carrageenan-induced rat paw test, the paw volume test and the abdominal constriction test (Tables 2 and 3).

In the first test, the intraplantar administration of carrageenan in the paw induces all typical inflammatory signs (i.e. paw swelling, hyperemia and hyperalgesia). Then, the selected compounds were administered at a dose of 20 mg/kg p.o. and the effect on the paw pressure tolerance and the volume of the paw were measured. All compounds showed a good activity against carrageenan-induced hyperalgesia 30 min after administration, disappearing almost completely at 2 h after treatment (Table 2). In particular, compound **10b** and its oxidized related molecule **11b** induced a tolerance higher than 53 g after 30 min from the treatment. However, while **10b** continues its significant activity even after 60 and 90 min, the pain tolerance induced by compound **11b** significantly decreases after 60 min. Moreover, a very good activity was demonstrated against carrageenan induced edema in the rat paw (Table 2), with a substantial complete remission in 1 h after the administration of all compounds at the same dose of 20 mg/kg p.o.

In the abdominal constriction test compounds **10a-c**, and **11b** were able to reduce the number of writhes in a statistically significant manner at the minimum dose of 20 mg/kg p.o., while at the dose of 10 mg/kg p.o., they were devoid of any antinociceptive efficacy (Table 3). Among these, a significant decrease of the writhing was highlighted by compound **10b**, in line with its higher potent affinity for the COX-2 isoform.

2.4. Molecular modeling studies

The aim of this computational study was threefold: a) to investigate the potential binding modes of such new class of inhibitors within the COX-2 binding site; b) to assess which, among sulfides **10**, sulfoxides **11**, and sulfones **12**, might be the real active compound or the inactive metabolite; c) to verify if the presence of S=O, or SO₂ functional group in the alkyl chain of 3-substituted 1,5-diarylpyrrole scaffold may have additional fruitful interactions within the binding site of COX-2 to maintain the selective inhibitory activity allowing at the same time to upgrade the structure-activity relationship (SAR) in this class of compounds and to confirm the bioisosteric suggestion.

In order to elucidate the inhibitor-enzyme interactions a molecular docking protocol has been used as described previously for alkoxyethyl ethers **9a-c**.^{21,26} In particular, we were aimed at understanding the influence of *n*-propyl chain in the binding modes of the newly conceived COX-2 selective inhibitors. Accordingly, each compound was docked into human COX-2 (*h*COX-2). To this end, Glide software with XP as scoring function was used for docking procedure along with *h*COX-2 enzyme (PDB ID: 5KIR) and compounds **10b**, **11b**, and **12b**.

Briefly, all the compounds showed a similar accommodation into *h*COX-2 binding site with comparable docking scores. In particular, the selected compounds showed the following docking scores: for **10b** we observed -7.97 kcal/mol of XPscore, for **11b** and **12b** the XPscores are -7.99 kcal/mol, and -7.61 kcal/mol, respectively. The comparable docking scores support similar potency in inhibiting the COX-2 enzyme in the low nanomolar range, although compound **10b** is the best inhibitor with an IC₅₀ of 0.011 μM. Regarding the docking outputs (Figure 2), all the compounds are able to interact with R513 by polar contacts and with Y355 and F518 by hydrophobic interactions. Moreover, compound **10b** can establish an additional H-bond with the backbone

of F518. Compounds **11b** and **12b** are not able to form the mentioned H-bonds due to the H-bonds network established by the side chains of Y355 and R120. These polar contacts led to a slight movement of the compounds into the binding site precluding the formation of the H-bond with the backbone of F518 since the distance is over 3 Å. Interestingly, the *n*-propyl moiety is well-tolerated by the enzyme observing its accommodation into a hydrophobic sub-pocket mainly composed by M113, Y115, V116, Y355, L531, L359. Although, the three compounds are able to accommodate the aliphatic chain into the mentioned sub-pocket we noted that the H-bonds formed from compounds **11b** and **12b** did not allow the *n*-propyl moiety to strongly interact with the above mentioned hydrophobic region, due to a different constrained conformation of this moiety, causing a weak interaction with respect to compound **10b**. This evidence is supported by the estimation of the Glide energy that provides a modified Coulomb-van der Waals interaction energy value taking into account the hydrophobic contribution to the binding. Compound **10b** possesses the most favourable Glide energy (-18.42 kcal/mol) over compounds **11b** and **12b** (-12.31 kcal/mol and -13.04 kcal/mol, respectively). This hydrophobic binding contribution could support the slight differences in COX-2 inhibition.

2.5. *In silico* prediction of potential sites of metabolism

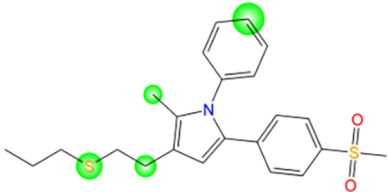
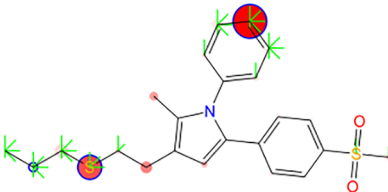
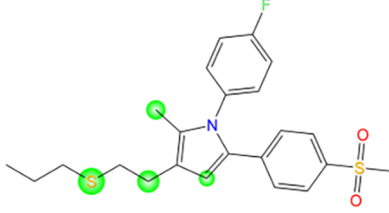
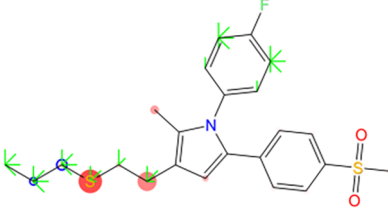
Despite the similar potency in COX-2 inhibition observed for compounds **10a** and **10b**, we noted a different efficacy when the compounds were tested *in vivo*. In particular, compound **10b** showed a superior anti-inflammatory and antinociceptive profile with respect to those found for **10a**. This different *in vivo* efficacy could be ascribable to the different metabolic stability of the compounds. In fact, we speculated that compound **10a** could be quickly metabolized contrarily to compound **10b**. This possibility prompted us to computationally investigate the differences in the sites of metabolism of the above-mentioned compounds. It is well established that cytochrome P450 enzymes are crucial in the metabolism of drugs. These heme-containing enzymes catalyze several reactions, including dealkylation, hydroxylation and double-bond oxidation, resulting in the degradation of compounds. The prediction of the sites of metabolism of drug-like molecules provides an overview of the metabolic stability of molecules, suggesting potential modification for the rational design of novel molecules with improved pharmacological profile. For this purpose we employed P450 site of metabolism (P450 SOM) application implemented in Schrödinger suite 2011. As demonstrated by some of us, this application is very useful in predicting potential soft spots aiming at understanding the liable sites of the molecules.³⁵ In particular, we predicted metabolism-mediated by isoforms CYP3A4, CYP2C9, and CYP2D6 of **10a** and **10b**. The prediction for isoforms CYP2C9 and CYP2D6 combined induced-fit docking (which determines accessibility of the compounds to the CYP reactive centre) with a rule-based approach to intrinsic reactivity. In the case of CYP3A4, which has a highly flexible binding site, only intrinsic reactivity was used to predict soft spots.^{36,37} The output of this *in silico* evaluation was reported in Table 4.

Based on the calculations, we speculate about the possibility that the mediated-metabolism of the mentioned molecules could be mainly determined by the isoforms CYP3A4 and CYP2C9 given that the calculation with the isoform CYP2D6 did not produce any results in terms of docking poses, denoting a lower affinity of these compounds for the CYP2D6 isoform. Concisely, compound **10a** is accommodated into CYP2C9 projecting the N₁-phenyl substituent towards the iron center of heme group (Figure 3). In particular, the *para* position of the mentioned substituent was found to be at only 3.8 Å, representing the main soft spots of the molecule. Accordingly, in this region relevant modifications of the molecule mediated by the heme-containing enzymes should occur.

The other soft spots in the sulfur chain could be less relevant in the metabolism of the compound **10a** since although the distances found between the potential soft spots in the chain and the reactive center are

Table 4

Results for prediction of sites of metabolism for studied compounds by P450 site of metabolism (P450 SOM) prediction workflow implemented in Schrödinger suite 2011.

Comp	CYP3A4 ^a	CYP2C9 ^b	CYP2D6 ^b
10a			no pose obtained ^c
10b			no pose obtained ^c

^a In the structure of each compound, atoms with the accessibility and the intrinsic reactivity for 3A4 are marked by green circles, in which the circle radius is proportional to the score. Larger scores mean higher reactivity.

^b In the structure of each compound, the Fe-accessibility of 2C9 and 2D6 are indicated by a set of green rays drawn out from the atom. The number of rays indicates the value of the Fe-accessibility, as determined by induced-fit docking. Each full-length ray represents one unit of accessibility, so the number of full-length rays is the integer part of the score. The remaining partial ray represents the decimal part of the score. The circles represent the overall score and the intrinsic reactivity. The radius of the circle corresponds to this score. The intensity of the red colour for each circle is proportional to the atomic intrinsic reactivity (the highest level of intrinsic reactivity was determined by dark red). A blue ring around the circle indicates that the atom passed through the CYP filtering stage. No ring indicates that the atom failed the CYP filtering stage.

^c the P450 SOM procedure did not found any poses into the isoforms and no compound-CYP2D6 complexes were formed.

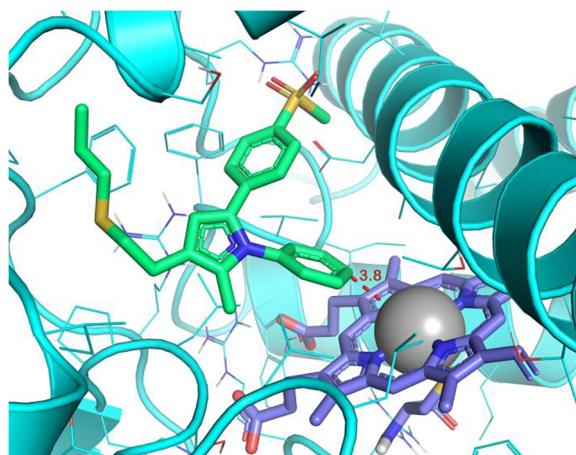


Figure 3. P450SOM docked pose of compounds **10a** (spring green sticks) into the CYP2C9 binding site (cyan cartoon). The binding site residues are represented by lines, the heme group is represented by light purple stick and the iron is represented by a grey sphere. The distance between the N₁-phenyl *para* position and the iron center is shown in red and the distance is expressed in Å. The picture was generated by PyMOL.

under 4 Å, the predicted accessibility to the iron reactive center is dramatically decreased with respect to the N₁-phenyl *para* position. On the contrary, the presence of the fluorine atom in **10b** was predicted to reduce CYP3A4- and CYP2C9-mediated metabolism leading to more stable analogues. In fact, as highlighted by the results reported in [Table 4](#) we can observe a dramatic decrease of the potential soft spots with a reduction of potential sites of metabolism. Accordingly, **10b** showed a significant decrease of the intrinsic reactivity for CYP3A4, and no relevant interactions with isoforms CYP2C9, and CYP2D6. The presented computational analysis supports the different *in vivo* efficacy representing one of the main reasons of the different anti-inflammatory/antinociceptive profile of the compound **10a** with respect

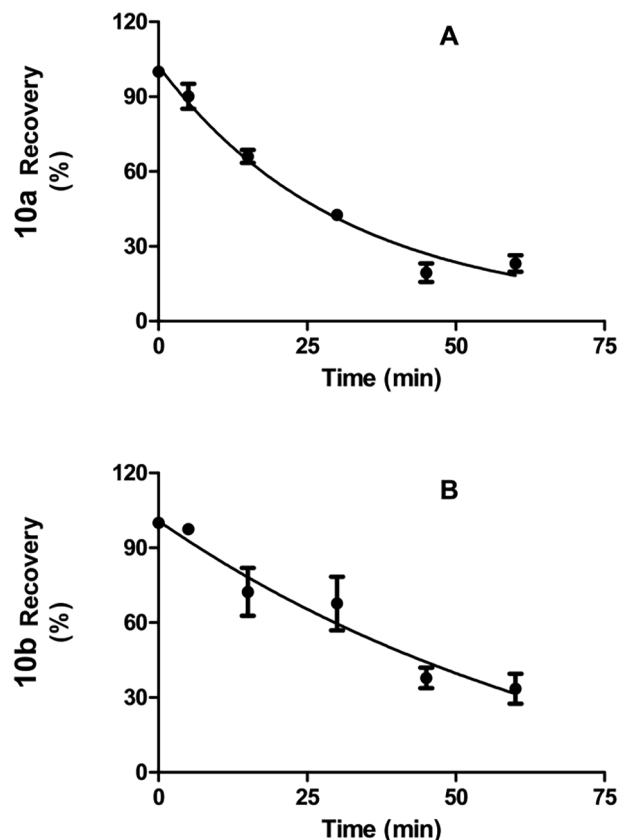


Figure 4. CYP-dependent metabolic depletion of 10 μM **10a** (A) and **10b** in human liver microsomal preparations. Results are presented graphically as percentage of compound recovery (100% at time 0 min) as a function of incubation time. Data are presented as mean ± sem, of three different experiments.

to compound **10b** in the presented animal models.

2.6. *In vitro* metabolic stability of **10a** and **10b** in human liver microsomes

In order to better explain experimentally the different efficacy in the *in vivo* studies and rationalize the computational predictions, the metabolic stability of compound **10a** and **10b** was assessed in human liver microsomal preparations. The plot of non-metabolized compound (%) versus time showed monoexponential decay relationship (Figure 4). The apparent decay constants k were 0.03245 min^{-1} and 0.0128 min^{-1} for **10a** and **10b**, respectively. The resulted half-life time and Cl_{int} were, respectively $t_{1/2} = 21.4$ and 54.15 min and $Cl_{int} = 58.3$ and $22.9 \mu\text{L}/\text{min}$, for **10a** and **10b**, respectively.

These results clearly indicate that compound **10a** should be considered moderate substrate of Cytochrome P450 system as resulted from its intrinsic clearance value. Interestingly the introduction of a fluorine in the molecule increased its metabolic stability. In fact the half-life time resulted more the two fold greater in the compound **10b**. The results suggest that both compounds can possess a favourable pharmacokinetic property, at least regarding their interaction with phase I enzyme system.

3. Conclusions

In summary, we have reported the design, synthesis, computational investigation and the biological evaluation based on *in vitro* and *in vivo* experiments of a novel series of 3-substituted 1,5-diarylpyrrole sulfur derivatives as COX-2 selective inhibitors endowed with anti-inflammatory/antinociceptive profile. In particular, the biological evaluation highlighted the strong inhibitory potency against the COX-2 enzyme in the low nanomolar range with no significant affinity against COX-1 with a remarkable selectivity ratio. Molecular modeling studies provided a detailed model of interaction into the COX-2 binding site for understanding the role of the different substituents introduced in lateral chain of the developed COX-2 selective inhibitors. Moreover, an extensive *in silico* investigation of the sites of metabolism of the molecules together with *in vitro* metabolic stability studies in human liver microsomes, allowed to propose one of the main reasons regarding the different *in vivo* potency observed for the compounds **10a** and **10b**. Overall, among the novel conceived derivatives, compound **10b** demonstrated the best efficacy in animal models of inflammatory pain over its congeneric compounds opening the way to the development of a novel anti-inflammatory and antinociceptive agent.

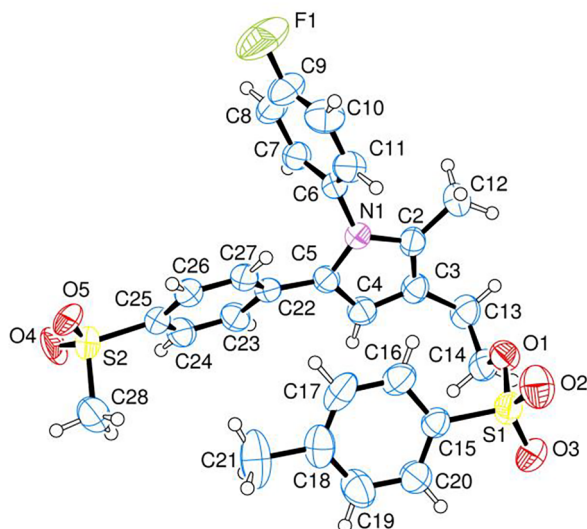


Figure 5. Crystallographic structure of compound **14b**. Ellipsoids enclose 50% probability.

4. Materials and methods

4.1. Chemistry

All chemicals used were of reagent grade. Yields refer to purified products and are not optimized. Melting points were determined in open capillaries on a Gallenkamp apparatus and are uncorrected. Merck silica gel 60 (230–400 mesh) was used for column chromatography. Merck TLC plates and silica gel 60 F₂₅₄ were used for TLC. ¹H- and ¹³C NMR spectra were recorded with a Bruker AC 400 spectrometer in the indicated solvent (TMS as internal standard). The values of the chemical shifts are expressed in ppm, and the coupling constants (J) are expressed in Hz. Mass spectra were recorded using an Agilent 1100 LC/MSD operating with an electrospray source. Purity of compounds **10a-c**, **11a,b**, and **12a,b** was assessed by RP-HPLC and was found to be higher than 95%. Merck LiChroCART® 125–4 C18 column was used in the HPLC analysis with acetonitrile–water–methanol (20:70:10) or acetonitrile–methanol (80:20) as the mobile phase at a flow rate of 1.0 mL/min. UV detection was achieved at 228 nm.

4.1.1. General procedure for the synthesis of tosylate derivatives **14a-c**.

To a solution of the suitable alcohol (**13a-c**)^{21,26} (1 equivalent) in CH₂Cl₂ (30 mL), 4-(dimethylamino)pyridine (DMAP) (1.5 equivalents) and *N,N*-diisopropylethylamine (DIPEA) (1.5 equivalents) were added in sequence. The solution was cooled at 0 °C, and tosyl chloride (1.5 equivalents) was added. After stirring for 3 h at room temperature, the reaction mixture was treated with water and the organic layer was washed with water, dried over anhydrous Na₂SO₄, filtered and evaporated *in vacuo*. The residue was purified by flash chromatography with the indicated eluent to obtain the expected tosyl derivative.

4.1.2. 2-(2-Methyl-5-(4-(methylsulfonyl)phenyl)-1-phenyl-1H-pyrrol-3-yl)ethyl-4-methylbenzene sulfonate (**14a**).

The title compound was obtained starting from the hydroxyl derivative **13a** (1.1 g, 3.28 mmol) as a light yellow solid (1.17 g, yield 70%) using petroleum ether–ethyl acetate (1:1 v/v) as the eluting mixture. ¹H NMR (400 MHz, CDCl₃) δ ppm: 1.98 (s, 3H), 2.40 (s, 3H), 2.84 (t, $J = 7.2$, 2H), 2.98 (s, 3H), 4.18 (t, $J = 7.2$, 2H), 6.30 (s, 1H), 7.08 (d, $J = 8.4$, 4H), 7.29 (d, $J = 7.6$, 2H), 7.38 (m, 3H), 7.62 (d, $J = 8.4$, 2H), 7.76 (d, $J = 8.0$, 2H). MS(ESI): m/z 510 (M + H⁺).

4.1.3. 2-(1-(3-Fluorophenyl)-2-methyl-5-(4-(methylsulfonyl)phenyl)-1H-pyrrol-3-yl)ethyl-4-methyl benzenesulfonate (**14b**).

The title compound was obtained starting from the hydroxyl derivative **13b** (0.74 g, 1.98 mmol) as a white solid (0.86 g, yield 82%, mp = 145.5–147.0 °C) using petroleum ether–ethyl acetate (7:3 v/v) as the eluting mixture. An X-ray quality analytical sample was obtained by recrystallization from dichloromethane by slow evaporation (Figure 5). ¹H NMR (400 MHz, CDCl₃) δ ppm: 1.98 (s, 3H), 2.41 (s, 3H), 2.84 (t, $J = 7.2$, 2H), 3.00 (s, 3H), 4.19 (t, $J = 7.2$, 2H), 6.30 (s, 1H), 7.09 (m, 6H), 7.30 (d, $J = 8.0$, 2H), 7.66 (d, $J = 8.4$, 2H), 7.77 (d, $J = 8.0$, 2H). MS(ESI): m/z 551 (M + Na⁺).

4.1.4. 2-(1-(4-Fluorophenyl)-2-methyl-5-(4-(methylsulfonyl)phenyl)-1H-pyrrol-3-yl)ethyl-4-methyl benzenesulfonate (**14c**).

The title compound was obtained starting from the hydroxyl derivative **13c** (0.41 g, 1.10 mmol) as a white solid (0.50 g, yield 86%) using petroleum ether–ethyl acetate (8:2 v/v) as the eluting mixture. ¹H NMR (400 MHz, CDCl₃) δ ppm: 2.00 (s, 3H), 2.41 (s, 3H), 2.84 (t, $J = 7.1$, 2H), 3.00 (s, 3H), 4.19 (t, $J = 7.2$, 2H), 6.31 (s, 1H), 6.84 (dd, $J = 9.1$, 2.0, 1H), 6.90 (d, $J = 7.9$, 1H), 7.13 (m, 3H), 7.31 (d, $J = 8.2$, 2H), 7.36 (m, 1H), 7.67 (d, $J = 8.3$, 2H), 7.77 (d, $J = 8.2$, 2H). MS(ESI): m/z 551 (M + Na⁺).

4.1.5. General procedure for the synthesis of alkyl sulfides **10a-c**.

To a solution of the appropriate tosyl derivative **14a-c** (1

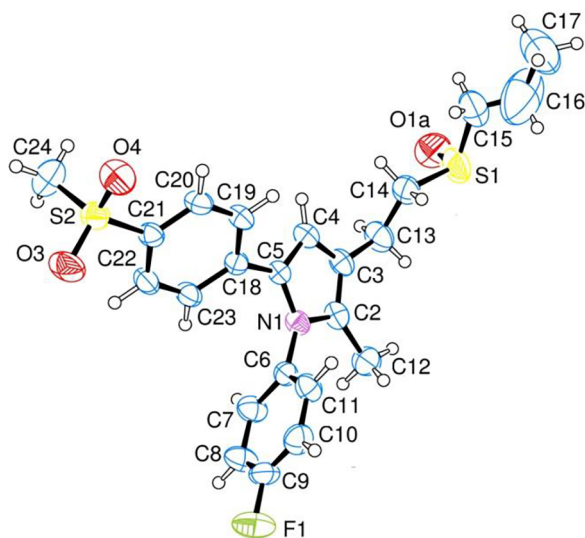


Figure 6. Crystallographic structure of compound **11b**. Ellipsoids enclose 50% probability.

equivalent) in anhydrous DMSO (15 mL), sodium 1-propanthiolate (1.5 equivalents) was added. The reaction mixture was stirred at room temperature under nitrogen atmosphere for 1 h, then diluted with water, and washed with ethyl acetate. The organic layer was dried over sodium sulfate, filtered and concentrated under reduce pressure. The residue was purified by flash chromatography using petroleum ether-ethyl acetate (7:3 v/v) as the eluting mixture.

4.1.6. 2-Methyl-5-(4-(methylsulfonyl)phenyl)-1-phenyl-3-(2-(propylthio)ethyl)-1H-pyrrole (10a).

The title compound was obtained starting from tosyl derivative **14a** (0.30 g, 0.59 mmol) as an off-white solid (0.17 g, yield 69%, mp = 107.5–108.5). ¹H NMR (400 MHz, CDCl₃) δ ppm: 0.99 (t, *J* = 7.2, 3H), 1.60–1.66 (m, 2H), 2.04 (s, 3H), 2.55 (t, *J* = 7.2, 2H), 2.75 (s, 4H), 2.96 (s, 3H), 6.43 (s, 1H), 7.12 (d, *J* = 8.4, 4H), 7.37 (m, 3H), 7.61 (d, *J* = 8.4, 2H). MS(ESI): *m/z* 414 (M + H⁺).

4.1.7. 1-(4-Fluorophenyl)-2-methyl-5-(4-(methylsulfonyl)phenyl)-3-(2-(propylthio)ethyl)-1H-pyrrole (10b).

The title compound was obtained starting from tosyl derivative **14b** (0.30 g, 0.57 mmol) as a white solid (0.20 g, yield 81%, mp = 111.5–113.5 °C). ¹H NMR (400 MHz, CDCl₃) δ ppm: 0.99 (t, *J* = 7.2, 3H), 1.64 (m, 2H), 2.03 (s, 3H), 2.55 (t, *J* = 7.2, 2H), 2.75 (s, 4H), 2.98 (s, 3H), 6.42 (s, 1H), 7.05–7.24 (m, 6H), 7.64 (d, *J* = 8.0, 2H). MS(ESI): *m/z* 432 (M + H⁺).

4.1.8. 1-(3-Fluorophenyl)-2-methyl-5-(4-(methylsulfonyl)phenyl)-3-(2-(propylthio)ethyl)-1H-pyrrole (10c).

The title compound was obtained starting from tosyl derivative **14c** (0.10 g, 0.19 mmol) as a white solid (0.070 g, yield 85%). ¹H NMR (400 MHz, CDCl₃) δ ppm: 0.99 (t, *J* = 7.4, 3H), 1.64 (m, 2H), 2.05 (s, 3H), 2.55 (t, *J* = 7.4, 2H), 2.74 (s, 4H), 2.98 (s, 3H), 6.42 (s, 1H), 6.87 (d, *J* = 8.8, 1H), 6.92 (d, *J* = 8.0, 1H), 7.09 (m, 1H), 7.14 (d, *J* = 8.0, 2H), 7.35 (m, 1H), 7.64 (d, *J* = 8.0, 2H). MS(ESI): *m/z* 432 (M + H⁺).

4.1.9. General procedure for the synthesis of sulfoxide (11a,b) and sulfone derivatives (12a,b).

To a solution of the appropriate sulfide (**10a,b**, 1 equivalent) in anhydrous dichloromethane (15 mL), a solution of *m*-CIPBA (2 equivalents) in CH₂Cl₂ (15 mL) was added slowly at 0 °C. The resulting mixture was stirred for 2 h at room temperature under a nitrogen atmosphere. The reaction mixture was washed with a saturated NaHCO₃

solution and then with water. The organic layer was dried over sodium sulfate, filtered, and concentrated under reduced pressure. The residue was purified by flash chromatography using petroleum ether-ethyl acetate (8:2) as eluent to obtain the sulfone derivative (**12a,b**) and then ethyl acetate to obtain the desired sulfoxide (**11a,b**) as the main product.

4.1.10. 2-Methyl-5-(4-(methylsulfonyl)phenyl)-1-phenyl-3-(2-(propylsulfonyl)ethyl)-1H-pyrrole (11a).

The title compound was obtained starting from sulfide derivative **10a** (0.10 g, 0.24 mmol) as a white solid (0.060 g, yield 58%). ¹H NMR (400 MHz, CDCl₃) δ ppm: 1.08 (t, *J* = 7.4, 3H), 1.78–1.87 (m, 2H), 2.06 (s, 3H), 2.58–2.78 (m, 2H), 2.97 (m, 7H), 6.42 (s, 1H), 7.12 (m, 4H), 7.37 (m, 3H), 7.62 (d, *J* = 8.4, 2H). MS(ESI): *m/z* 430 (M + H⁺).

4.1.11. 1-(4-Fluorophenyl)-2-methyl-5-(4-(methylsulfonyl)phenyl)-3-(2-(propylsulfonyl)ethyl)-1H-pyrrole (11b).

The title compound was obtained starting from sulfide derivative **10b** (0.10 g, 0.23 mmol) as a white solid (0.066 g, yield 62%, mp = 174.0–175.0 °C). An analytical sample was obtained by recrystallization from ethyl acetate by slow evaporation (Figure 6). ¹H NMR (400 MHz, CDCl₃) δ ppm: 1.08 (t, *J* = 7.4, 3H), 1.80–1.92 (m, 2H), 2.05 (s, 3H), 2.60–3.11 (m, 9H), 6.42 (s, 1H), 7.03–7.14 (m, 6H), 7.64 (d, *J* = 8.4, 2H). MS(ESI): *m/z* 448 (M + H⁺).

4.1.12. 2-Methyl-5-(4-(methylsulfonyl)phenyl)-1-phenyl-3-(2-(propylsulfonyl)ethyl)-1H-pyrrole (12a).

The title compound was obtained as a secondary product from the reaction mixture of compound **11a** as an off-white solid (0.010 g, yield 10%). ¹H NMR (400 MHz, CDCl₃) δ ppm: 1.06 (t, *J* = 7.2, 3H), 1.88 (m, 2H), 2.06 (s, 3H), 2.91 (m, 2H), 2.99–3.07 (m, 5H), 3.21 (m, 2H), 6.39 (s, 1H), 7.09–7.13 (m, 4H), 7.39 (m, 3H), 7.64 (d, *J* = 8.8, 2H). MS (ESI): *m/z* 446 (M + H⁺).

4.1.13. 1-(4-Fluorophenyl)-2-methyl-5-(4-(methylsulfonyl)phenyl)-3-(2-(propylsulfonyl)ethyl)-1H-pyrrole (12b).

The title compound was obtained as a secondary product from the reaction mixture of compound **11b** as an off-white solid (0.010 g, yield 9%, mp = 158.5–162.0 °C). ¹H NMR (400 MHz, CDCl₃) δ ppm: 1.06 (t, *J* = 7.2, 3H), 1.86 (m, 2H), 2.05 (s, 3H), 2.92 (m, 2H), 2.99–3.07 (m, 5H), 3.20 (m, 2H), 6.38 (s, 1H), 7.08–7.14 (m, 6H), 7.66 (d, *J* = 8.4, 2H). MS(ESI): *m/z* 464 (M + H⁺).

4.2. Pharmacology. In vitro anti-inflammatory study.

The *in vitro* profiles of compounds **10a-c**, **11a,b**, and **12a,b**, related to their inhibitory activity toward both COX-1 and COX-2 isoenzymes were evaluated through a cell-based assay employing murine monocyte/macrophage J774 cell lines. The cell line was grown in DMEM supplemented with 2 mM glutamine, 25 mM HEPES, 100 units/mL penicillin, 100 µg/mL streptomycin, 10% fetal bovine serum (FBS), and 1.2% sodium pyruvate. Cells were plated in 24-well culture plates at a density of 2.5 × 10⁵ cells/mL or in 60 mm diameter culture dishes (3 × 10⁶ cells per 3 mL per dish) and allowed to adhere at 37 °C in 5% CO₂ for 2 h. Immediately before the experiments, the culture medium was replaced with fresh medium and cells were stimulated as previously described.³⁸ The evaluation of COX-1 inhibitory activity was achieved by pre-treating cells with the test compounds (10 µM) for 15 min and then incubating them at 37 °C for 30 min with 15 µM arachidonic acid to activate the constitutive COX. For the compounds with COX-1% inhibition higher than 50% (at 10 µM), the cells were also treated with lower concentrations (0.1–1 µM). At the end of the incubation, the supernatants were collected for the measurement of prostaglandin E₂ (PGE₂) levels by a radioimmunoassay (RIA). To evaluate COX-2 activity, the cells were stimulated for 24 h with *Escherichia coli* lipopolysaccharide (LPS, 10 µg/mL) to induce COX-2, both

in the absence and in the presence of the test compounds (0.01–10 μM). Celecoxib was used as a reference compound for the selectivity index. The supernatants were collected for the measurement of PGE2 by means of RIA.

4.3. *In vivo* anti-inflammatory and antinociceptive study.

In vivo anti-inflammatory activity of the title compounds was also assessed and performed as follows:

4.3.1. Animals.

Male Swiss albino mice (23–25 g) and Sprague–Dawley or Wistar rats (150–200 g) were used. Fifteen mice and four rats were housed per cage. The cages were placed in the experimental room 24 h before the test for acclimatization. The animals were fed with a standard laboratory diet and tap water *ad libitum* and kept at $23 \pm 1^\circ\text{C}$ with a 12 h light/dark cycle, light on at 7 a.m. All experiments were carried out in accordance with the NIH Guide for the Care and Use of Laboratory Animals. All efforts were made to minimize animal suffering and to reduce the number of animals used.

4.3.2. Paw-pressure test

The paw-pressure test was performed by inducing an inflammatory process by the intraplantar (i.pl.) carrageenan (0.1 mL, 1%) administration 4 h before the test. The nociceptive threshold in the rat was determined with an analgesimeter, according to the method described by Leighton *et al.*³⁹ Threshold pressure was measured before and 30, 60, and 120 min after treatment. An arbitrary cut-off value of 250 g was adopted.

4.3.3. Carrageenan-induced edema.

The carrageenan-induced paw edema test was also performed. Rat paw volumes were measured using a plethysmometer. Four hours after the injection of carrageenan (0.1 mL injection of 1.0%), the paw volume of the right hind paw was measured and compared with saline/carrageenan treated controls. Rats received test compounds 3 h 30 min after carrageenan. The results are reported as paw volume expressed in mL.

4.3.4. Antinociceptive assay.

Antinociceptive activity was determined by means of an intraperitoneal (i.p.) injection of a 0.6% acetic acid (10 mL/kg) induced writhing in the mouse abdominal constriction test according to Koster.⁴⁰ The number of stretching movements was counted for 10 min, starting 5 min after acetic acid injection.

4.4. Analysis of *in vitro* metabolic stability of 10a and 10b in human liver microsomes

Compounds **10a** and **10b**, dissolved in ACN, was incubated at 37°C , separately at 10 μM concentration in 100 mM phosphate buffer (pH 7.4) with 0.48 mg/mL human as previously reported.⁴¹ Enzymatic reactions were started by addition of a NADPH-regenerating system (2 mM NADPH), 10 mM glucose-6-phosphate, 0.4 U/ml glucose-6-phosphate dehydrogenase). Reactions were terminated at regular time intervals (overall range 0–60 min) by adding a double volume of acetonitrile. All incubations were performed in triplicate. HPLC analysis was performed on Agilent 1100 Series liquid chromatography system equipped with a Merck LiChroCART® 250–4,6 and coupling with UV–VIS detector, setting at λ 234 nm. Analysis was carried out using gradient elution of a binary solution; eluent A was ACN (acetonitrile), while eluent B consisting of an aqueous solution of formic acid (0.1%). The analysis started at 0% A for three minutes, then rapidly increased up to 98% in 12 min and finally remaining at 98% A until 18 min. The analysis was performed at flow rate of 0.8 mL min^{-1} and injection volume was 20 μL . The intrinsic clearance (Clint) was calculated by the equation:

$$\text{Clint} = k(\text{min}^{-1}) \times [V]/[P]$$

where k is the rate constant for the depletion of substrate, V is the volume of incubation in μL and P is the amount of microsomal proteins as reported elsewhere.⁴²

4.5. Computational details

4.5.1. Ligands and protein preparation

The hCOX-2 crystal structure (PDB ID: 5KIR)⁴³ was taken from protein data bank and prepared by Protein Preparation Wizard (PPW) protocol (Maestro suite 2011) for obtaining suitable structures for molecular docking calculations as previously reported.^{44,45} Water molecules and compounds used in the crystallization process were removed. PPW protocol performed a series of computational steps to: (1) add hydrogens, (2) optimize the orientation of hydroxyl groups, Asn, and Gln, and the protonation state of His, and (3) perform a constrained minimization refinement with the *impre* utility. The refined proteins were used in molecular docking calculation as reported in the next paragraph. The 3D structures of ligands were built in Maestro 9.2 (Schrödinger, LLC, New York, NY, 2011). MacroModel software was used for the energy minimizations employing the OPLS-2005 force field. The solvent effects were simulated using the analytical Generalized-Born/Surface-Area (GB/SA) model⁴⁶ and no cut-off for nonbonded interactions was selected. Polak-Ribiere conjugate gradient (PRCG) method with 1000 maximum iterations and 0.001 gradient convergence threshold was employed. All compounds reported in this paper were treated by LigPrep application (LigPrep version 2.5, Schrödinger, LLC, New York, NY, 2011) in order to generate the most probable ionization state at cellular pH (7.4 ± 0.2) as reported by us.^{47–49}

4.5.2. Molecular docking

Glide software (Glide, version 5.7, Schrödinger, LLC, New York, NY, 2011) has been employed to perform the docking studies presented in this paper, using the ligands and proteins prepared as above-mentioned, applying Glide extra precision (XP) scoring function.^{50,51} Energy grids were prepared using default value of protein atom scaling factor (1.0 Å) within a cubic box centered on the crystallized ligand (Rofecoxib). After grid generation, the ligands were docked into the enzymes. The number of poses entered to post-docking minimization was set to 50. Glide XP score was evaluated. In order to assess the validity of docking protocol, compounds crystallized with hCOX-2 were used as reference compounds (rofecoxib from 5KIR,⁴³ salicylic acid from 5F1A,⁵² meclorfenamic acid from 5IKQ,⁵³ mefenamic acid from 5IKR,⁵³ tolfenamic acid from 5IKT,⁵³ and flufenamic acid from 5IKV⁵³) for a re-docking procedure. The docking results revealed a similar accommodation for the above mentioned reference compounds with respect to the crystal structures with low RMSD (data not shown).

4.5.3. P450 site of metabolism

Compounds **10a** and **10b** were evaluated for their potential sites of metabolism by P450 site of metabolism (P450 SOM) workflow (P450 Site of Metabolism Prediction, version 1.1, Schrödinger, LLC, New York, NY, 2011) implemented in Schrödinger suite 2011.³⁵ For each molecule P450 SOM performed a calculation of intrinsic reactivity coupled to induced-fit docking (IFD) (Schrödinger Suite 2011; Induced Fit Docking protocol; Glide version 5.7, Schrödinger, LLC, New York, NY, 2011; Prime version 3.0, Schrödinger, LLC, New York, NY, 2011) for the selected isoform of cytochrome. The reactivity rules have been parameterized in P450 SOM to predict atomic reactivity profiles for promiscuous P450 enzymes that are thought to be mostly independent of structural restrictions on the binding poses. The reactivity is predicted with a linear free energy approach based on the Hammett and Taft scheme, where the reactivity of a given atom is the sum of a baseline reactivity rate and a series of perturbations determined by the connectivity.³⁷ The induced-fit docking approach is a variation on the

normal protocol. The initial sampling is enhanced by generating multiple starting conformations, so that a wider range of poses is found in the initial docking stage. The initial docking includes van der Waals scaling of the receptor and alanine mutation of the most flexible residues. In the Prime refinement step, any residue with an atom within 5 Å of any ligand pose is selected for side-chain prediction. The subsequent minimization includes the ligand, side chains, and backbones of the flexible residues. The ligand is then redocked into each of the low-energy protein conformations, determined by a 40 kcal/mol cut-off. There is no final scoring stage, because all poses are considered in determining which atoms are sufficiently accessible to the reactive heme iron. Any atom within the cut-off distance of 5 Å from the heme iron is considered as a potential site of metabolism.³⁷

4.6. X-Ray crystallography

Single crystals of **11b** and **14b** were submitted to X-ray data collection on an Oxford-Diffraction Xcalibur Sapphire 3 (Santa Clara, CA, USA) diffractometer with a graphite monochromated Mo-K α radiation ($\lambda = 0.71073$ Å) at 293 K. The structures were solved by direct methods implemented in SHELXS-2013 program.⁵⁴ The refinements were carried out by full-matrix anisotropic least-squares on F2 for all reflections for non-H atoms by means of the SHELXL-2018 program.⁵⁵ Crystallographic data (excluding structure factors) for the structure in this paper have been deposited with the Cambridge Crystallographic Data Centre as supplementary publications no. CCDC 1,881,112 (**11b**), and 1,881,113 (**14b**). Copies of the data can be obtained, free of charge, on application to CCDC, 12 Union Road, Cambridge CB2 1EZ, UK; (fax: +44(0)-1223-336-033; or e-mail: deposit@ccdc.cam.ac.uk).

Author contribution

S.B., M.P., A.Cap. M.A. wrote the paper; A.Rea., A.Chel., M.P., A.G., A.D.C., G.Giu., synthesized the compounds; S.B., G.C. performed the computational studies; G.Gio. performed the X-ray studies; M.V. carried out the analysis of *in vitro* metabolic stability in human liver microsomes; L.S., A.Ros., S.P., C.L.M., L.D.C.M., E.L., C.G. performed the *in vitro* and *in vivo* pharmacological studies; M.A. designed and coordinated the work.

Declaration of Competing Interest

The authors declare that they have no known competing financial interests or personal relationships that could have appeared to influence the work reported in this paper.

Acknowledgements

The authors wish to thank Dr. Francesco Berrettini (University of Siena) for X-ray acquisition data.

Appendix A. Supplementary data

Supplementary data to this article can be found online at <https://doi.org/10.1016/j.bmc.2019.115045>.

References

- Silverstein FE, Faich G, Goldstein JL, et al. Gastrointestinal toxicity with celecoxib vs nonsteroidal anti-inflammatory drugs for osteoarthritis and rheumatoid arthritis: the CLASS study: a randomized controlled trial. *Celecoxib Long-term Arthritis Safety Study*. *JAMA*. 2000;284:1247–1255.
- Hawkey C, Laine L, Simon T, et al. Comparison of the effect of rofecoxib (a cyclooxygenase 2 inhibitor), ibuprofen, and placebo on the gastroduodenal mucosa of patients with osteoarthritis: a randomized, double-blind, placebo-controlled trial. The Rofecoxib Osteoarthritis Endoscopy Multinational Study Group. *Arthritis Rheum*. 2000;43:370–377.
- Arico S, Pattingre S, Bauvy C, et al. Celecoxib induces apoptosis by inhibiting 3-phosphoinositide-dependent protein kinase-1 activity in the human colon cancer HT-29 cell line. *J Biol Chem*. 2002;277:27613–27621.
- Sawaoka H, Kawano S, Tsuji S, et al. Cyclooxygenase-2 inhibitors suppress the growth of gastric cancer xenografts via induction of apoptosis in nude mice. *Am J Physiol*. 1998;274:G1061–G1067.
- Liu XH, Kirschenbaum A, Yao S, Lee R, Holland JF, Levine AC. Inhibition of cyclooxygenase-2 suppresses angiogenesis and the growth of prostate cancer *in vivo*. *J Urol*. 2000;164:820–825.
- Davies G, Martin LA, Sacks N, Dowsett M. Cyclooxygenase-2 (COX-2), aromatase and breast cancer: a possible role for COX-2 inhibitors in breast cancer chemoprevention. *Ann Oncol*. 2002;13:669–678.
- Kargman SL, O'Neill GP, Vickers PJ, Evans JF, Mancini JA, Jothy S. Expression of prostaglandin G/H synthase-1 and -2 protein in human colon cancer. *Cancer Res*. 1995;55:2556–2569.
- Pasinetti GM. Cyclooxygenase and Alzheimer's disease: implications for preventive initiatives to slow the progression of clinical dementia. *Arch Gerontol Geriatr*. 2001;33:13–28.
- Fitzgerald GA, Patrono C. The coxibs, selective inhibitors of cyclooxygenase-2. *N Engl J Med*. 2001;345:433–442.
- Bohm HJ, Flohr A, Stahl M. Scaffold hopping. *Drug Discov. Today Technol*. 2004;1:217–224.
- Penning TD, Talley JJ, Bertenshaw SR, et al. Synthesis and biological evaluation of the 1,5-diarylpyrazole class of cyclooxygenase-2 inhibitors: identification of 4-[5-(4-methylphenyl)-3-(trifluoromethyl)-1H-pyrazol-1-yl]benzene nesulfonamide (SC-58635, celecoxib). *J Med Chem*. 1997;40:1347–1365.
- Riendeau D, Percival MD, Brideau C, et al. Etoricoxib (MK-0663): preclinical profile and comparison with other agents that selectively inhibit cyclooxygenase-2. *J Pharmacol Exp Ther*. 2001;296:558–566.
- Prasit P, Wang Z, Brideau C, et al. The discovery of rofecoxib, [MK 966, Vioxx, 4-(4-methylsulfonylphenyl)-3-phenyl-2(5H)-furanone], an orally active cyclooxygenase-2-inhibitor. *Bioorg Med Chem Lett*. 1999;9:1773–1778.
- Talley JJ. Selective inhibitors of cyclooxygenase-2 (COX-2). *Prog Med Chem*. 1999;36:201–234.
- Grosser T, Fries S, FitzGerald GA. Biological basis for the cardiovascular consequences of COX-2 inhibition: therapeutic challenges and opportunities. *J Clin Invest*. 2006;116:4–15.
- Hernandez-Diaz S, Varas-Lorenzo C, Garcia Rodriguez LA. Non-steroidal antiinflammatory drugs and the risk of acute myocardial infarction. *Basic Clin Pharmacol Toxicol*. 2006;98:266–274.
- Rodriguez LA, Patrignani P. The ever growing story of cyclo-oxygenase inhibition. *Lancet*. 2006;368:1745–1747.
- Fries S, Grosser T, Price TS, et al. Marked interindividual variability in the response to selective inhibitors of cyclooxygenase-2. *Gastroenterology*. 2006;130:55–64.
- Biava M, Porretta GC, Poce G, et al. Cyclooxygenase-2 inhibitors. 1,5-diarylpyrrol-3-acetic esters with enhanced inhibitory activity toward cyclooxygenase-2 and improved cyclooxygenase-2/cyclooxygenase-1 selectivity. *J Med Chem*. 2007;50:5403–5411.
- Di Bari L, Pescitelli G, Salvadori P, et al. Synthesis, resolution, and absolute configuration of two novel and selective cyclooxygenase-2 inhibitors based on the 1,5-diarylpyrrole structure. *Tetrahedron-Asymmetry*. 2006;17:3430–3436.
- Anzini M, Rovini M, Cappelli A, et al. Synthesis, biological evaluation, and enzyme docking simulations of 1,5-diarylpyrrole-3-alkoxyethyl ethers as selective cyclooxygenase-2 inhibitors endowed with anti-inflammatory and antinociceptive activity. *J Med Chem*. 2008;51:4476–4481.
- Biava M, Porretta GC, Poce G, et al. Novel analgesic/anti-inflammatory agents: diarylpyrrole acetic esters endowed with nitric oxide releasing properties. *J Med Chem*. 2011;54:7759–7771.
- Anzini M, Di Capua A, Valenti S, et al. Novel analgesic/anti-inflammatory agents: 1,5-diarylpyrrole nitrooxyalkyl ethers and related compounds as cyclooxygenase-2 inhibiting nitric oxide donors. *J Med Chem*. 2013;56:3191–3206.
- Fioravanti A, Tinti L, Pascarelli NA, et al. In vitro effects of VA441, a new selective cyclooxygenase-2 inhibitor, on human osteoarthritic chondrocytes exposed to IL-1 β . *J Pharmacol Sci*. 2012;120:6–14.
- Sticozzi C, Belmonte G, Cervellati F, et al. Antiproliferative effect of two novel COX-2 inhibitors on human keratinocytes. *Eur J Pharm Sci*. 2013;49:133–141.
- Di Capua A, Sticozzi C, Brogi S, et al. Synthesis and biological evaluation of fluorinated 1,5-diarylpyrrole-3-alkoxyethyl ether derivatives as selective COX-2 inhibitors endowed with anti-inflammatory activity. *Eur J Med Chem*. 2016;109:99–106.
- Cheleschi S, Calamia V, Fernandez-Moreno M, et al. In vitro comprehensive analysis of VA692 a new chemical entity for the treatment of osteoarthritis. *Int Immunopharmacol*. 2018;64:86–100.
- Cotton FA, Wilkinson G, Gaus PL. *Basic Inorganic Chemistry*. J. Wiley; 1995.
- Ilardi EA, Vitaku E, Njardarson JT. Data-mining for sulfur and fluorine: an evaluation of pharmaceuticals to reveal opportunities for drug design and discovery. *J Med Chem*. 2014;57:2832–2842.
- Brunell D, Sagher D, Kesaraju S, Brot N, Weissbach H. Studies on the metabolism and biological activity of the epimers of sulindac. *Drug Metab Dispos*. 2011;39:1014–1021.
- He M, Rettie AE, Neal J, Trager WF. Metabolism of sulfinpyrazone sulfide and sulfinpyrazone by human liver microsomes and cDNA-expressed cytochrome P450s. *Drug Metab Dispos*. 2001;29:701–711.
- Smith K, Small A, Hutchings MG. Regiospecific Synthesis of Alpha-Alkoxy-1-Alkyl-1,2,4-Triazoles and Alpha-Alkylthio-1-Alkyl-1,2,4-Triazoles from Aldehydes and Glyoxals. *Synlett*. 1991;485–486.
- K.-M. Roy, Sulfoxes and Sulfoxides, 2000.
- Trautmann M, Lubahn S, Holdt HJ. Preparation, characterisation and properties of

- sulphoxide modified polystyrene resins for solid-phase extraction of Pt-IV, Ru-III and Ru-IV from hydrochloric acid. *React Funct Polym.* 2014;83:84–97.
35. Gemma S, Camodeca C, Sanna Coccone S, et al. Optimization of 4-aminoquinoline/clotrimazole-based hybrid antimalarials: further structure-activity relationships, in vivo studies, and preliminary toxicity profiling. *J Med Chem.* 2012;55:6948–6967.
 36. Sherman W, Day T, Jacobson MP, Friesner RA, Farid R. Novel procedure for modeling ligand/receptor induced fit effects. *J Med Chem.* 2006;49:534–553.
 37. Friesner RA, Banks JL, Murphy RB, et al. Glide: a new approach for rapid, accurate docking and scoring. 1. Method and assessment of docking accuracy. *J Med Chem.* 2004;47:1739–1749.
 38. Rossi A, Ligresti A, Longo R, Russo A, Borrelli F, Sautebin L. The inhibitory effect of propolis and caffeic acid phenethyl ester on cyclooxygenase activity in J774 macrophages. *Phytomedicine.* 2002;9:530–535.
 39. Leighton GE, Rodriguez RE, Hill RG, Hughes J. kappa-Opioid agonists produce antinociception after i.v. and i.c.v. but not intrathecal administration in the rat. *Br J Pharmacol.* 1988;93:553–560.
 40. Koster R, Anderson M, D.B. E.J. Acetic Acid for Analgesic Screening. *Fed. Proc.* 1959;18:412–418.
 41. D'Elia P, De Matteis F, Dragoni S, Shah A, Sgaragli G, Valoti M. DP7, a novel dihydropyridine multidrug resistance reverter, shows only weak inhibitory activity on human CYP3A enzyme(s). *Eur J Pharmacol.* 2009;614:7–13.
 42. Williamson B, Wilson C, Dagnell G, Riley R.J. Harmonised high throughput microsomal stability assay. *J Pharmacol Toxicol Methods.* 2017;84:31–36.
 43. Orlando BJ, Malkowski MG. Crystal structure of rofecoxib bound to human cyclooxygenase-2. *Acta Crystallogr. F Struct. Biol. Commun.* 2016;72:772–776.
 44. Brindisi M, Maramai S, Gemma S, et al. Development and Pharmacological Characterization of Selective Blockers of 2-Arachidonoyl Glycerol Degradation with Efficacy in Rodent Models of Multiple Sclerosis and Pain. *J Med Chem.* 2016;59:2612–2632.
 45. Giovani S, Penzo M, Butini S, et al. Plasmodium falciparum subtilisin-like protease 1: discovery of potent difluorostatone-based inhibitors. *RSC Adv.* 2015;5:22431–22448.
 46. Still WC, Tempczyk A, Hawley RC, Hendrickson T. Semianalytical Treatment of Solvation for Molecular Mechanics and Dynamics. *J Am Chem Soc.* 1990;112:6127–6129.
 47. Brindisi M, Gemma S, Kunjir S, et al. Synthetic spirocyclic endoperoxides: new antimalarial scaffolds. *MedChemComm.* 2015;6:357–362.
 48. Brindisi M, Maramai S, Brogi S, et al. Development of novel cyclic peptides as proapoptotic agents. *Eur J Med Chem.* 2016;117:301–320.
 49. Brogi S, Giovani S, Brindisi M, et al. In silico study of subtilisin-like protease 1 (SUB1) from different Plasmodium species in complex with peptidyl-difluorostatones and characterization of potent pan-SUB1 inhibitors. *J Mol Graph Model.* 2016;64:121–130.
 50. Brindisi M, Cavella C, Brogi S, et al. Phenylpyrrole-based HDAC inhibitors: synthesis, molecular modeling and biological studies. *Future Med Chem.* 2016;8:1573–1587.
 51. Zaccagnini L, Brogi S, Brindisi M, et al. Identification of novel fluorescent probes preventing PrP(Sc) replication in prion diseases. *Eur J Med Chem.* 2017;127:859–873.
 52. Lucido MJ, Orlando BJ, Vecchio AJ, Malkowski MG. Crystal Structure of Aspirin-Acetylated Human Cyclooxygenase-2: Insight into the Formation of Products with Reversed Stereochemistry. *Biochemistry.* 2016;55:1226–1238.
 53. Orlando BJ, Malkowski MG. Substrate-selective Inhibition of Cyclooxygenase-2 by Fenamic Acid Derivatives Is Dependent on Peroxide Tone. *J Biol Chem.* 2016;291:15069–15081.
 54. Sheldrick GM. A short history of SHELX. *Acta Crystallogr. A.* 2008;64:112–122.
 55. Sheldrick GM. Crystal structure refinement with SHELXL. *Acta Crystallogr. C Struct. Chem.* 2015;71:3–8.